Chinese Chemical Letters 34 (2023) 108059

Contents lists available at ScienceDirect

Chinese Chemical Letters

journal homepage: www.elsevier.com/locate/cclet

Magnetorheological elastomer and smartphone enable microfluidic biosensing of foodborne pathogen

Gaozhe Cai[a,b,1], Yuhe Wang[a,1], Yingchao Zhang[a], Lingyan Zheng[c], Jianhan Lin[a,*]

[a] Key Laboratory of Agricultural Information Acquisition Technology, Ministry of Agriculture and Rural Affairs, China Agricultural University, Beijing 100083, China

[b] State Key Laboratory of Transducer Technology, Shanghai Institute of Microsystem and Information Technology, Chinese Academy of Sciences, Shanghai 200050, China

[c] Beijing Engineering and Technology Research Center of Food Additives, Beijing Technology & Business University (BTBU), Beijing 100048, China

ARTICLE INFO

Article history:
Received 16 May 2022
Revised 28 November 2022
Accepted 10 December 2022
Available online 13 December 2022

Keywords:
Magnetorheological elastomer
Microfluidic chip
Colorimetric biosensor
Bacterial detection
Smartphone image processing

ABSTRACT

Rapid detection of foodborne pathogens is crucial to prevent the outbreaks of foodborne diseases. In this work, we proposed a novel microfluidic biosensor based on magnetorheological elastomer (MRE) and smartphone. First, micropump and microvalves were constructed by deforming the MRE under magnetic actuation and integrated into the microfluidic biosensor for fluidic control. Then, the micropump was used to deliver immune porous gold@platinum nanocatalysts (Au@PtNCs), bacterial sample, and immunomagnetic nanoparticles (MNPs) into a micromixer, where they were mixed, incubated and magnetically separated to obtain the Au@PtNC-bacteria-MNP complexes. After 3,3′,5,5′-tetramethylbenzidine and hydrogen peroxide were injected and catalyzed by the Au@PtNCs, smartphone was used to measure the color of the catalysate for quantitative analysis of target bacteria. Under optimal conditions, this biosensor could detect *Salmonella typhimurium* quantitatively and automatically in 1 h with a linear detection range of 8.0×10^1 CFU/mL to 8.0×10^4 CFU/mL and a detection limit of 62 CFU/mL. The microfluidic biosensor was compact in size, simple to use, and efficient for detection, and might be used for in-field screening of foodborne pathogens to prevent food poisoning.

Foodborne diseases have been a serious threat to human health and global economy [1,2]. Illnesses from foodborne pathogens such as *Salmonella* and *Escherichia coli* account for most cases of diarrhea and raise the requirement for early detection of foodborne pathogens in foods [3,4]. For the detection of foodborne pathogens, various methods have been explored, including culture (the gold standard), enzyme-linked immunosorbent assay (ELISA), and polymerase chain reaction (PCR). The conventional culture approach is highly sensitive, but requires one day of culture in biosafety level 2 laboratory and two days to obtain results [5]. Because of their high sensitivity and short time, nucleic acid-based PCR techniques have become popular, however they still need complex nucleic acid extraction [6]. Antibody-antigen based ELISA methods are fast and high-throughput, however they are often faced with insufficient sensitivity [7]. Therefore, bacterial detection methods with shorter detection time, higher sensitivity and simpler operation are urgently required to ensure food safety.

With rapid advance of nanotechnology, biosensors are being developed as a cutting-edge diagnostic tool for rapid and sensitive detection of pathogens and have been widely applied in food safety [8]. However, many biosensors were costly because they often relied on expensive equipment and skilled personnel [9,10], which limited their applications in bacterial detection. In recent years, smartphone based microfluidic biosensors have emerged as an interdisciplinary technology by combining optical biosensors, microfluidic chips and smartphone Apps to provide new approaches for bacterial detection, and have shown their merits of automatic operation, compact size and high sensitivity [11–13]. Reis *et al.* [14] proposed a smartphone-based microfluidic fluorescence sandwich immunoassay to detect *E. coli* with a detection limit of 240 CFU/mL. Pan *et al.* [15] developed a microfluidic colorimetric biosensor for detection of *Salmonella* using thiolated polystyrene microspheres to aggregate gold nanoparticles and a smartphone imaging APP to monitor colorimetric signals with a detection limit of 60 CFU/mL.

The fluidic control in microfluidic chips mainly depends on external pumps or valves connected with the chips through tubing [16], which may cause cross contaminations and greatly hinder

* Corresponding author.
E-mail address: jianhan@cau.edu.cn (J. Lin).
[1] These authors contributed equally to this work.

https://doi.org/10.1016/j.cclet.2022.108059
1001-8417/

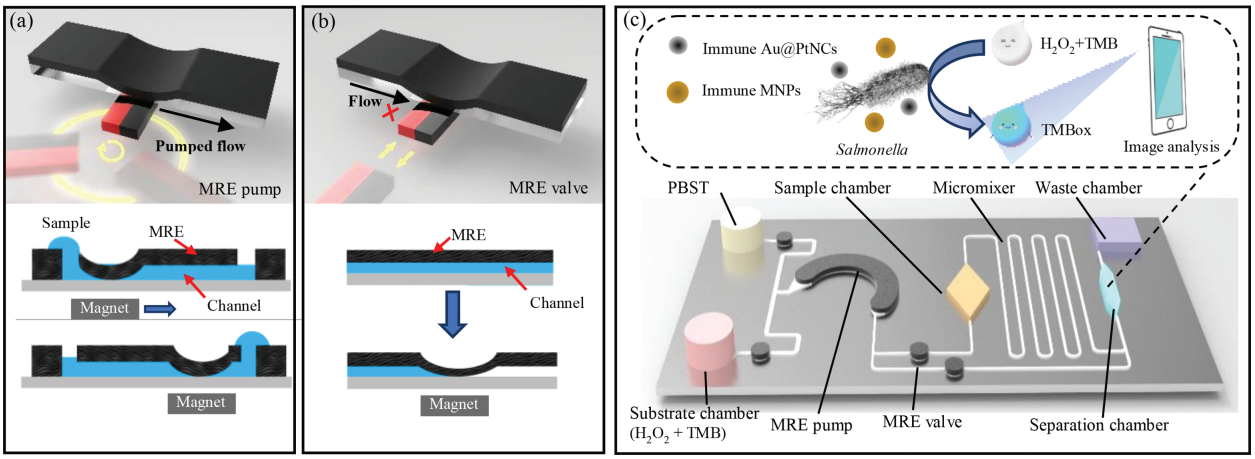

Scheme 1. (a) The principle of the MRE micropump. (b) The principle of the MRE microvalve. (c) The schematic diagram of the microfluidic biosensor for rapid and sensitive detection of *Salmonella typhimurium*.

their on-site applications. To address this issue, numerous on-chip micropumps and microvalves have been developed to realize automatic fluidic control without the need of any external connection [17,18]. Microfluidic chips are generally divided into passive and active. In passive chips, capillary force was often used for fluidic control based on surface tension effect generated by the geometry or surface chemical properties of microchannels [19,20]. It is not difficult to manufacture a passive chip, however it requires hydrophilic and hydrophobic treatment on some parts of the microchannels, and more importantly, it is a great challenge to adjust the flow rate and flow direction. Active chips often depend on different external energy sources to drive the fluids, such as piezoelectric [21], electrostatic [22], pneumatic [23], and acoustic [24]. Although their fluidic control is more flexible, it is hard to integrate the bulky and complicated external sources onto the chips. Hence, the development of on-chip micropumps and microvalves is essential for microfluidic biosensors.

Magnetorheological elastomer (MRE) is a composite material consisting of nonmagnetic polymeric matrix and micro-sized ferromagnetic particles, which can be precisely controlled by a magnetic field [25–27]. MRE can be applied onto a microfluidic chip for fluidic control by altering a magnetic field as it offers unique advantages including low cost, easy fabrication, repeated use, and tunable mechanical properties. Li *et al.* [28] proposed the MRE-based micromixer by bonding the MRE membrane with a thickness of 100 μm to a cavity-structured polydimethylsiloxane (PDMS) channel. The fluid was controlled by squeezing the MRE membrane with an electromagnet to form an active micromixer. Zhang *et al.* [29] proposed the MRE-based artificial cilium (350 μm in length and 50 μm in diameter) to drive the fluid in the microfluidic chip. The fluidic control method based on MRE membrane and artificial cilium performed small driving force, making it unable to overcome the pressure drop in the microfluidic chip for large-volume samples.

Hence, we developed a simple microfluidic biosensor based on MRE and smartphone for automatic detection of *Salmonella typhimurium*. As illustrated in Schemes 1a and b, a high gradient magnetic field was rotated using a stepper motor to induce periodic deformation of a semi-circle MRE membrane to form the MRE pump, and each MRE valve was constructed using an electromagnet to deform MRE membrane and thus block the channel. Further, a microfluidic chip integrated with MRE microvalves and micropump was developed. As shown in Scheme 1c, the mixture of immune porous gold@platinum nanocatalysts (Au@PtNCs), bacteria sample and immune magnetic nanoparticles (MNPs) was preloaded in the diamond sample chamber by pipetting, followed by mixing in the micromixer and incubation and magnetic separation in the separation chamber to form Au@PtNC-bacteria-MNP complexes using the MRE pump, MRE valves and magnet. After the preloaded hydrogen peroxide and 3,3′,5,5′-tetramethylbenzidine (TMB) were transferred from the substrate chamber to the separation chamber, the peroxidase mimic enzyme property of the Au@PtNCs allowed them to catalyze TMB to produce a variety of colors in the chamber, which was measured using the smartphone App for quantitative analysis of the target bacteria.

This microfluidic chip was the key to this biosensor and fabricated using 3D printed molds, poly(dimethoxy)silane (PDMS) and iron microparticles. As shown in Fig. S1 (Supporting information), the PDMS mold (for these microchannels and chambers) and the MRE molds (for MRE pump and valve) were first printed using a 3D printer (Objet 30 Pro Stratasystem), and the MRE molds were attached to the PDMS mold with double-sided tape (thickness: 100 μm) after they were washed with alcohol. Then, the mixture of PDMS prepolymer and curing agent (ratio 10:1) was poured into the PDMS mold and cured at 65 °C overnight. After peeling off the MRE molds and double-sided tapes, the mixture of PDMS prepolymer, curing agent and iron microparticles (diameter: 2-5 μm) at the mass ratio of 30:1:30 was poured and cured at 65 °C overnight. Finally, the whole PDMS channel with the MRE membranes was peeled from the PDMS mold and bonded to a glass plate after oxygen plasma treatment.

As a result, one MRE pump and four MRE valves were developed on this microfluidic chip according to this fabrication process. The MRE pump mainly relied on the periodic deformation of the MRE channel under the action of a rotating magnetic field to squeeze the fluid in the microfluidic chip. To make it more suitable for the rotation of the magnetic field, the MRE channel was designed as a circular arc (height: 100 μm, internal diameter: 8 mm, external diameter: 13 mm, angle: 180°). The MRE molds, the PDMS mold and the fabricated MRE pump were illustrated in Fig. S2 (Supporting information). To induce the periodic deformation of the MRE micropump, a rotating magnetic field was designed and developed by placing multiple permanent magnets (9 mm × 4 mm × 3 mm) in six holes on a 3D-printed circular holder (diameter: 38 mm, thickness: 8 mm). In this paper, three magnet layouts (Fig. S3a in Supporting information) were developed and their performance to drive the MRE pump was compared. Three magnet layouts were termed as Single Magnet (SM), Dual Repelling Magnets (DRM) and Dual Attractive Magnets (DAM), respectively. A stepper motor was used to rotate the magnet holder, and its speed

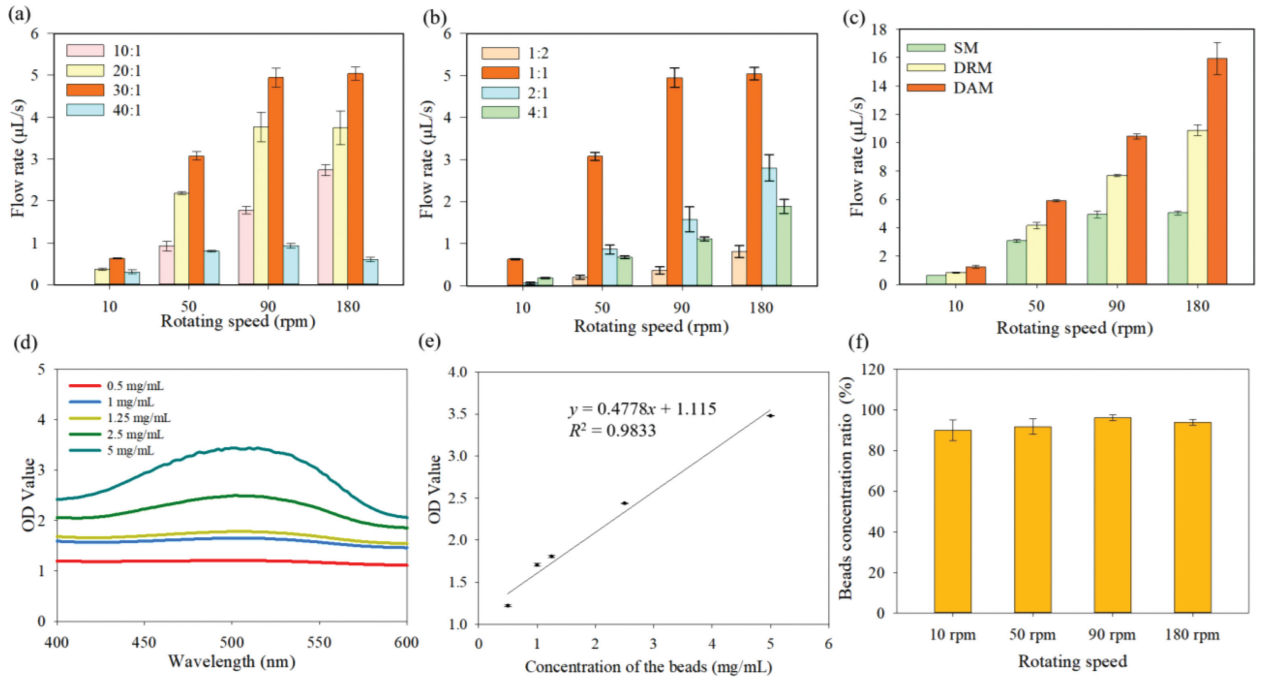

Fig. 1. Optimization of the MRE pump. Influence of (a) mass ratio between the PDMS prepolymer and the curing agent, (b) mass ratio between the iron microparticles and the mixture of the PDMS prepolymer and the curing agent, and (c) different magnet layouts (the optimized parameter was marked in orange). Relationship between (d) the wavelength and the OD value, (e) concentration of polystyrene microparticles and OD value at 505 nm, and (f) rotating speed and bead concentration ratio of the outlet to inlet.

and direction were controlled by an Arduino microcontroller *via* the smartphone and motor driver.

The performance of the MRE membrane has an important impact on the microfluidic pump and valve, which were directly influenced by the ratio of the iron microparticles, the PDMS prepolymer and the curing agent. Thus, different mass ratios of the PDMS mixture (PDMS prepolymer and curing agent) were used to manufacture the MRE pump and driven by the rotating magnetic field at different speeds to evaluate their performance. When the MRE pump was turned on to continuously transfer deionized water from the inlet, it was collected from the outlet every minute and the volume was measured to calculate the flow rate. As shown in Fig. 1a, the increase on mass ratio of PDMS prepolymer and curing agent from 10:1 to 30:1 resulted in a higher flow rate. However, when the mass ratio further increased to 40:1, the flow rate dropped dramatically. It was believed that the elasticity of the MRE membrane deteriorated at the ratio of 40:1 and the MRE membrane could not return to its original state, resulting in a reduction in flow rate. Furthermore, as the speed for magnetic field rotation changed from 10 rpm to 90 rpm, the flow rate increased from 0.6 μL/s to 5 μL/s. This was because the increase on the rotating speed led to the increase on more pumping times. When the speed further increased to 180 rpm, there was no significant increase on flow rate. This was because the magnetic response time of MRE membrane was insufficient at this speed. Thus, the optimal ratio of the prepolymer and curing agent was set as 30:1 for this work. Besides, different mass ratios of the iron microparticles to the PDMS mixture (1:2, 1:1, 2:1 and 4:1) were further prepared for manufacturing the MRE membrane to investigate the performance of the MRE pump. As shown in Fig. 1b, the highest fluid rate of 5 μL/s was observed at the mass ratio of 1:1. The lower mass ratio of the iron microparticles to the PDMS mixture (1:2) might result in weaker magnetic force on the MRE membrane by the rotating magnetic field and thus worse magnetic response, while the higher mass ratio (2:1 and higher) might lead to poorer flexibility and thus worse magnetic response. The operation and performance of the MRE pump could be found in Video S1 (Supporting information).

The rotating magnetic field was also crucial to the MRE pump. Thus, three magnet layouts (SM, DRM and DAM) were used to generate magnetic fields and rotated by the stepper motor. The flow rate was used as the index to evaluate the performance of the MRE pump driven by the different magnet layouts. As shown in Fig. 1c, the best performance was observed using DAM layout, which had the highest flow rate compared to the SM and DRM layouts and more importantly, exhibited a good linear relationship between the flow rate and the rotating speed. This was due to the high-gradient magnetic field generated by these two attractive magnets induced the sufficient periodic deformation of the MRE membrane. To further explain the phenomena, COMSOL Multiphysics 5.3a software was used to simulate the three layouts of magnetic fields. As shown in Fig. S3b, the maximum magnetic field intensity of the magnetic field generated by the DAM layout was 0.9 T, which was higher than that of the SM layout (0.7 T). In addition, the attenuation rate of the magnetic field by the DAM layout at the range of 30-40 mm was significantly larger than that of the DRM layout, indicating the DAM layout had a higher gradient than the DRM one and thus resulting in a faster MRE membrane deformation. Therefore, the DAM layout was chosen to construct the magnetic field for driving the MRE membrane in this work.

The MRE pump was realized through the deformation of the MRE membrane by the rotating magnetic field for periodic extrusion on the MRE-PDMS channel. Due to its strong hydrophobicity, the MRE-PDMS channel might suffer from nonspecific adsorption. Hence, the non-specific adsorption test was carried out using the red polystyrene microparticles having a similar size (1 μm) with the target bacteria (1-3 μm). Prior to test, the relationship between the concentration and OD value of the polystyrene microparticles was first built for the subsequent experiments (Figs. 1d and e), and 1% BSA (Bovine Serum Albumin) was used to block the MRE-PDMS channel for 30 min. The polystyrene microparticles were pumped at different flow rates and their OD values at 502 nm were col-

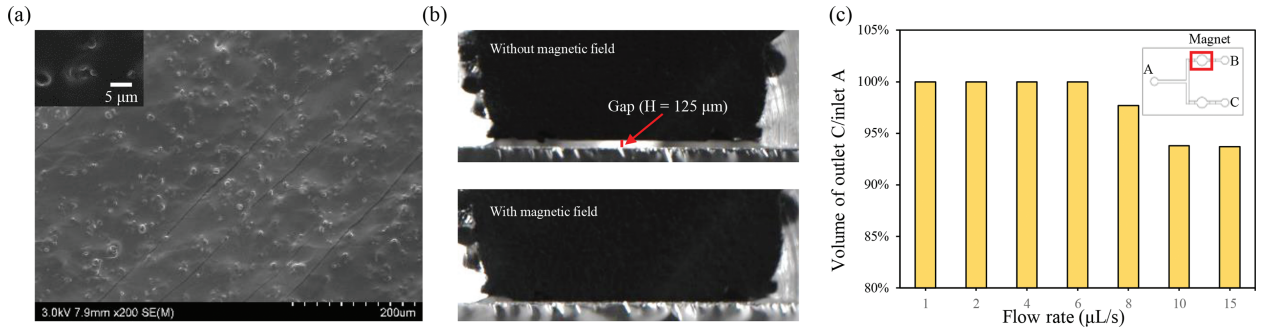

Fig. 2. Optimization of the mechanical properties of MRE valve. (a) The SEM image of the iron microparticles in PDMS. (b) The gap without and with magnetic field. (c) The sealing effect of different flow rates.

lected from the inlet and outlet. As shown in Fig. 1f, this MRE pump had no obvious nonspecific adsorption after BSA blocking.

The MRE valve was developed by applying a magnetic field with a high gradient and high intensity to cause the deformation of the MRE membrane to block the microfluidic channel. The channel of the MRE valve was designed as a circular chamber (height: 100 μm, internal diameter: 4 mm). To test its performance more accurately, a microfluidic chip, consisting of a main channel connected with an inlet and two sub-channels connected with two MRE valves, was developed. The mold of the MRE valve and the fabricated MRE chip were illustrated in Fig. S4 (Supporting information). The driver for the MRE valve (Fig. S4e) consisted of two parts: (1) a 3D-printed holder with one rectangular hole (10.3 mm × 4.1 mm × 4 mm) for placing two permanent magnets (10 mm × 2 mm × 4 mm) in a mutual repelling layout, and (2) an electromagnet (input voltage: 12 V) with a metal rod for pulling and pushing the magnet holder by the Arduino and smartphone. The function of the MRE valve was mainly realized using the high gradient magnetic field to induce the deformation of the MRE membrane. The distribution of the iron microparticles in MRE membrane could directly affect the performance of the MRE valve, and thus was observed by scanning electron microscope (SEM). As shown in Fig. 2a, the iron microparticles were evenly distributed in the membrane, indicating the uniform mechanical and magnetic properties. Furthermore, the leak proof performance was very important for the MRE valve. To ensure no leak at the close condition, the change of the cross-section of the MRE-PDMS channel at the presence of the high gradient magnetic field was photographed by the camera to observe the deformation of the MRE membrane. Fig. 2b showed that there was no obvious gap between the MRE membrane and the glass substrate in the presence of the high gradient magnetic field. To further investigate the performance of this MRE valve, 500 μL of PBS solution was injected into the chip at different flow rates, and the electromagnet was turned on and placed under the MRE valve at the sub-channel connected with outlet C, followed by collecting the PBS solution at both outlets (B and C). The ratio of the volume collected at outlet C to the volume injected from inlet A was used as the index to evaluate the valving performance of the MRE valve. When the flow rate was no more than 6 μL/s, the MRE valve performed admirably, as illustrated in Fig. 2c. Nonetheless, when the flow rate exceeded 6 μL/s, partial PBS solution flowed out from outlet B due to the increase on the pressure in the chip, indicating that the maximum flow rate of this MRE valve was 6 μL/s.

The MRE pump and valves were integrated into the microfluidic chip for automatic detection of foodborne pathogens. The detailed design of the microfluidic chip was shown in Fig. S5a (Supporting information). Briefly, two inlets connected with the MRE valves were designed as open chambers (diameter: 10 mm) for adding PBST, TMB and H_2O_2. A rhombic sample chamber (total volume: 100 μL) for storing the mixture of the bacterial sample, the immune MNPs and the immune Au@PtNCs was placed behind the MRE pump. The synthesis of the immune Au@PtNCs could be found in Supporting information. Two holes on the top of the chamber for injecting samples were sealed by a scotch tape after the sample was loaded. The bacterial sample, the immune MNPs and the immune Au@PtNCs were mixed and incubated by a serpentine micromixer and separated by a magnet on a separation chamber. For flexible control of the MRE pump and valves, a magnetic control system was developed using the Arduino, the Bluetooth module and the smartphone. This control system consisted of: (1) a bracket (Fig. S5b) with three PMMA boards for placing the microfluidic chip, rotating the magnetic field and housing the electromagnets, (2) a control circuit (Fig. S6 in Supporting information) for driving and controlling the rotating magnetic field and electromagnets, and (3) a smartphone App (Fig. S7 in Supporting information) for data analysis and result display. The working sequence of this MRE based microfluidic chip was shown in Fig. S9 (Supporting information).

To evaluate the bacterial detection performance of this biosensor, parallel tests on *Salmonella typhimurium* with different concentrations from 8×10^1 CFU/mL to 8×10^6 CFU/mL in the sterile PBS were conducted under the optimal conditions. Transmission electron microscope (TEM) imaging was performed to confirm the successful forming of the MNP-*Salmonella*-Au@PtNC complexes (Fig. 3a). Fig. 3b indicated that the saturation value obtained by the smartphone App increased from 20 to 240 when the concentration of the bacteria changed from 8×10^1 CFU/mL to 8×10^6 CFU/mL. A linear relationship between saturation (S) and concentration (C) was obtained and calculated as $S = 6.2066\ln(C) - 6.7847$ ($R^2 = 0.981$). The detection limit for the biosensor was calculated to be 62 CFU/mL based on three times of signal-to-noise ratio.

To investigate the specificity of this biosensor, *Salmonella typhimurium*, *E. coli* O157:H7, *Salmonella derby*, *Salmonella enteritidis* and *Listeria monocytogenes* and their mixture at the concentration of 8×10^5 CFU/mL were tested. As shown in Fig. 3c, the non-target bacteria showed obviously lower saturation than the target bacteria and were close to the negative control. In addition, the saturation of the mixture containing all the bacteria was close to that of the target bacteria. These results demonstrated that this biosensor had great specificity for *Salmonella typhimurium*.

To further demonstrate the feasibility of the biosensor for the detection of *Salmonella typhimurium* in real food samples, parallel tests on spiked chicken samples were conducted. The spiked samples were prepared according to China's food safety national standards. Briefly, 25 g of chicken breast was first added into 225 mL of PBS and homogenized for 2 min using a stomacher. After standing for 5 min, the supernatant was then collected. Finally, *Salmonella typhimurium* was added into the supernatant to obtain the spiked chicken samples with the bacteria concentrations from

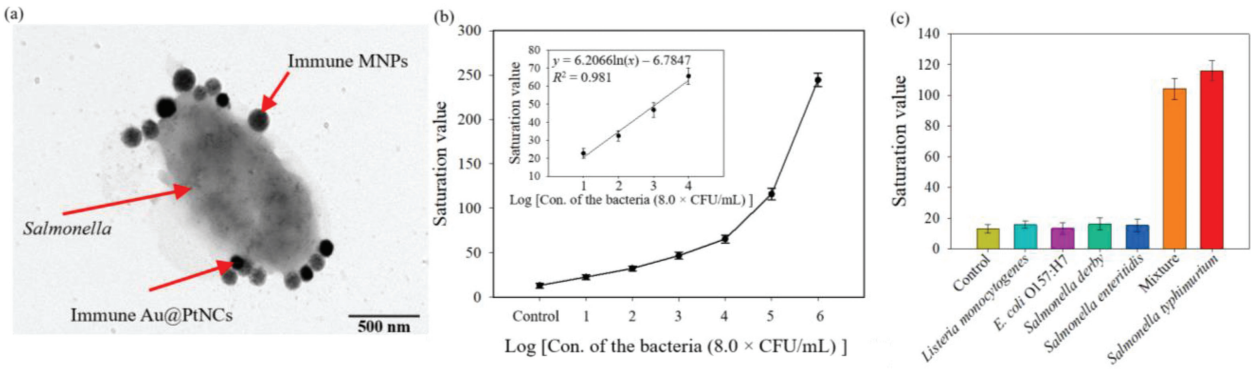

Fig. 3. (a) The TEM image of the MNP-*Salmonella*-Au@PtNC complexes. (b) The saturation value of different concentrations of the bacteria. (c) The specificity for different bacteria.

0.8×10^2 CFU/mL to 0.8×10^5 CFU/mL. As shown in Table S1 (Supporting information), the recoveries of the chicken sample ranged from 98.67% to 108.37% with a standard deviation from 6.79% to 9.21%. The mean recovery was 103.12%, indicating that this biosensor exhibited good feasibility for the detection of *Salmonella typhimurium* in chicken samples.

In summary, a microfluidic biosensor integrating the MRE micropump and microvalves was proposed for rapid and automatic detection of *Salmonella*. The MRE micropump and valves were able to automatically and precisely control the fluids inside this microfluidic chip without any external connection and could effectively avoid the cross-contamination caused by the external pumps in the traditional microfluidic control. Combined with smartphone and Arduino, the integration of sample pretreatment, bacterial detection and signal processing in the detection of foodborne pathogens was realized automatically. The microfluidic biosensor was proved to detect *Salmonella* as low as 62 CFU/mL within 1 h. Compared with the recently reported works for foodborne pathogen detection (Table S2 in Supporting information), this microfluidic biosensor behaved better in the convenience and sensitivity with a shorter or comparable detection time, and showed great potential for on-site detection of pathogens in food supply chains due to its integration, automation, and simplicity.

Declaration of competing interest

The authors report no declarations of interest.

Acknowledgments

This study was supported by Walmart Foundation (No. UA2020-154). The authors would like to thank Walmart Food Safety Collaboration Center for their great support.

Supplementary materials

Supplementary material associated with this article can be found, in the online version, at doi:10.1016/j.cclet.2022.108059.

References

[1] J.K. Liu, B. Li, W.W. Li, et al., Front. Med. 12 (2017) 48–57.
[2] U. Ryan, N. Hijjawi, L. Xiao, Int. J. Parasitol. 48 (2018) 1–12.
[3] U.C. Nze, M.G. Beeman, C.J. Lambert, et al., Biosens. Bioelectron. 135 (2019) 137–144.
[4] O. Ehuwa, A.K. Jaiswal, S. Jaiswal, Foods 10 (2021) 907.
[5] F. Carvalho, J. George, H.M.A. Sheikh, R. Selvin, J. Biomed. Nanotechnol. 14 (2018) 829–846.
[6] A. Ahmed, J.V. Rushworth, N.A. Hirst, P.A. Millner, Clin. Microbiol. Rev. 27 (2014) 631–646.
[7] S. Kumar, K. Balakrishna, H. Batra, Biomed. Environ. Sci. 21 (2008) 137–143.
[8] J.d.D. Habimana, J. Ji, X. Sun, Anal. Lett. 51 (2018) 2933–2966.
[9] Y. Liu, D. Jiang, S. Wang, et al., Chin. Chem. Lett. 33 (2022) 3156–3160.
[10] Z. Xu, X. Jiang, S. Liu, M. Yang, Chin. Chem. Lett. 31 (2020) 185–188.
[11] D. Xu, X. Huang, J. Guo, X. Ma, Biosens. Bioelectron. 110 (2018) 78–88.
[12] S.C. Kim, U.M. Jalal, S.B. Im, S. Ko, J.S. Shim, Sensor. Actuator. B: Chem. 239 (2017) 52–59.
[13] G. Xing, W. Zhang, N. Li, Q. Pu, J. Lin, Chin. Chem. Lett. 33 (2021) 1743–1751.
[14] I.P. Alves, N.M. Reis, Biosens. Bioelectron. 145 (2019) 111624.
[15] Y. Man, M. Ban, A. Li, et al., Food Chem. 354 (2021) 129578.
[16] M. Jie, S. Mao, H. Li, J. Lin, Chin. Chem. Lett. 28 (2017) 1625–1630.
[17] M. Boyd-Moss, S. Baratchi, M. Di Venere, K. Khoshmanesh, Lab Chip 16 (2016) 3177–3192.
[18] C.D. Chin, V. Linder, S.K. Sia, Lab Chip 12 (2012) 2118–2134.
[19] R. Safavieh, D. Juncker, Lab Chip 13 (2013) 4180–4189.
[20] L. Xu, A. Wang, X. Li, K.W. Oh, Biomicrofluidics 14 (2020) 031503.
[21] X. He, R. Bian, N. Lin, et al., Microsyst. Technol. 25 (2019) 2637–2647.
[22] V. Varghese, R. Padmanabhan, IJBBR 3 (2020) 182–187.
[23] M. Park, T.S. Seo, Biosens. Bioelectron. 126 (2019) 405–411.
[24] A.A. Doinikov, M.S. Gerlt, A. Pavlic, J. Dual, Microfluid. Nanofluid. 24 (2020) 1–13.
[25] Y. Li, J. Li, W. Li, H. Du, Smart Mater. Struct. 23 (2014) 123001.
[26] A.K. Bastola, M. Hossain, Compos. Part B: Eng. 200 (2020) 108348.
[27] A.K. Bastola, M. Paudel, L. Li, W. Li, Smart Mater. Struct. 29 (2020) 123002.
[28] J. Li, M. Zhang, L. Wang, et al., Microfluid. Nanofluid. 10 (2011) 919–925.
[29] S. Zhang, Y. Wang, R. Lavrijsen, P.R. Onck, J.M. den Toonder, Sensor. Actuator. B: Chem. 263 (2018) 614–624.